Formation of U-shaped diamond trenches with vertical {111} sidewalls by anisotropic etching of diamond (110) surfaces

M. Nagai[a], Y. Nakamura[a], T. Yamada[a], T. Tabakoya[a,b], T. Matsumoto[a,c], T. Inokuma[a], C.E. Nebel[c,d], T. Makino[b], S. Yamasaki[b,c], N. Tokuda[a,b,c,*]

[a] Graduate School of Natural Science and Technology, Kanazawa University, Kanazawa, Ishikawa 920-1192, Japan
[b] Advanced Power Electronics Research Center, National Institute of Advanced Industrial Science and Technology (AIST), Tsukuba, Ibaraki 305-8568, Japan
[c] Nanomaterials Research Institute, Kanazawa University, Kanazawa, Ishikawa 920-1192, Japan
[d] Fraunhofer-Institute for Applied Solid State Physics (IAF), Tullastraße 72, Freiburg 79108, Germany

ABSTRACT

U-shaped diamond trenches with vertical {111} sidewalls for power devices were successfully obtained by anisotropic etching of diamond (110) surfaces using Ni films in high-temperature (1000 °C) water vapor. The etching rate for the diamond (110) surfaces was estimated to be 3.8 μm/min on the basis of the relationship between etching time and etching depth of diamond trenches with (110) bottoms. These (110) bottoms gradually disappeared as the etching progressed. Finally, they completely vanished and each diamond trench was surrounded by four vertical {111} sidewalls and two slanted {111} sidewalls. The formation mechanisms of the U-shaped diamond trenches are also discussed on the basis of the experimental results.

1. Introduction

Diamond has excellent physical, electrical, and mechanical properties [1]. Therefore, its application as a semiconductor in various devices, including power devices, quantum devices, and microelectromechanical systems (MEMS) has been expected [2–12]. To fabricate these devices, a diamond etching technique for forming device structures is indispensable. Conventionally, almost all diamond device structures have been constructed by top-down plasma etching. However, for the conventional semiconductor Si, device structures are also fabricated by wet chemical etching with crystal anisotropies [13–17]. In such crystal anisotropic etching, the etching rate for the (111) planes is much lower than those for the other planes [18,19]. Accordingly, the shapes of trenches formed by the anisotropic etching are governed by angles of the {111} planes with respect to the surface to be etched [20–24]. To increase the number of feasible diamond device structures, the crystal anisotropic etching technique for diamond is also important. However, wet chemical etching cannot be simply applied to diamond because of its chemical inertness.

A more sophisticated etching technique that uses hydrogen plasma is available; however, the etching rate is low and selective etching is difficult because of the difficulty of mask selection [25–27]. However, diamond etching using Ni films in high-temperature water vapor, which

we have developed as a non-plasma diamond etching technique in recent years, has crystal anisotropy and high selectivity [28]. Moreover, the etching process has the highest etching rate reported for diamond (100) surfaces. It can also generate atomically flat diamond (111) regions [28,29]. It therefore has strong potential for use in diamond device processing. However, because of the angle of the {111} planes with respect to the surface to be etched, forming U-shaped diamond trenches with vertical sidewalls on diamond (100) or (111) surfaces is difficult. Such U-shaped diamond trenches are strongly required, especially for diamond metal-oxide-semiconductor field-effect transistors (MOSFETs) because the U-shaped trench structure enables a lower on-resistance than other MOSFET structures as a consequence of its higher channel density [1,30,31].

When Si (110) is subjected to crystal anisotropic wet chemical etching, U-shaped Si trenches with vertical {111} sidewalls are formed because of the presence of {111} planes perpendicular to the (110) surface [22]. Therefore, U-shaped diamond trenches with vertical {111} sidewalls can be formed on diamond (110) surfaces via diamond etching using Ni films in high-temperature water vapor [28,29].

In this paper, we report the formation of U-shaped diamond trenches with vertical {111} sidewalls via the anisotropic etching of diamond (110) surfaces using Ni films in high-temperature water vapor. The formation mechanisms of the U-shaped diamond trenches are

discussed in detail.

2. Material and methods

High-pressure–high-temperature synthetic IIa-type single-crystal diamond (110) substrates were used. First, the substrates were immersed into H_2SO_4/H_2O_2 (1:2) at 120 °C for 15 min to remove surface contaminants. Second, circular Ni films were formed on the substrate photolithographically. The thickness and diameters of the circular Ni films were 0.2 μm and 100, 200, and 300 μm, respectively. Third, the samples were annealed on a quartz plate in a quartz tube at 1000 °C in an electric furnace for 1, 8, and 15 min in the presence of water vapor. The ramp rates of the temperature in the furnace were 20 °C/min from room temperature to 800 °C and 10 °C/min from 800 °C to 1000 °C. The water vapor was generated by bubbling 400 sccm of N_2 gas through ultrapure water. This annealing is hereafter referred to as "water-vapor annealing." Finally, the samples were immersed in a hot mixed acid of H_2SO_4/HNO_3 (3:1) at 220 °C for 20 min to remove the deposited films.

The morphology of the sample surfaces was observed and characterized by laser microscopy (LM) using a laser microscope (LEXT OLS4100, Olympus) and scanning electron microscopy (SEM) using a scanning electron microscope (S-4500, Hitachi).

3. Results and discussion

Fig. 1 shows three-dimensional (3D) LM height images of the sample surface morphology (a) after deposition of a Ni film with a diameter of 100 μm onto the diamond (110) surface and (b) after water-vapor annealing at 1000 °C for 15 min and removal of the deposited film. The diamond under the deposited Ni film was selectively etched, and a diamond trench was formed. The etching mechanism was discussed in our previous paper [28]. The shape of the trench was hexagonal on the diamond (110) surface, and its maximum depth was ~39 μm.

Fig. 2 shows a two-dimensional (2D) LM height image of the surface morphology at the same location represented in Fig. 1(b). Fig. 2(b) and (c) depicts cross-sectional images corresponding to the line segments AA' and BB' in Fig. 2(a), respectively. The line segments AA' and BB' in Fig. 2(a) were along the ⟨100⟩ and ⟨111⟩ directions, respectively. Regarding the middle line of the diamond trench in the (110) direction, the cross-sectional image corresponding to the line segment symmetric to the line segment BB' is equivalent to that corresponding to the line segment BB'. The protrusion structures near the top and bottom of the diamond trench are due to noise (see Fig. 3). Fig. 2 shows that the trench was surrounded by six sidewalls and that four of them intersected the (110) surface vertically on four straight lines in the ⟨112⟩ directions (hereafter referred to as "vertical sidewalls"); the other two sidewalls crossed the (110) surface at an angle of ~35° on two straight

lines in the ⟨110⟩ directions (hereafter referred to as "slanted sidewalls"). This arrangement crystallographically indicates that the six sidewalls were {111} planes. Therefore, we conclude that a U-shaped diamond trench with vertical {111} sidewalls can be obtained by anisotropic etching of diamond (110) surfaces using Ni films in high-temperature water vapor. The slanted {111} sidewalls also intersected the other sidewalls at an angle of ~110°, immediately below the center line between the two tangents in the < 110 > direction. Because all of the diamond trench was surrounded by the {111} sidewalls, it can be seen that the {111} planes functioned as etching stopping planes. Thus, the etching rate for the {111} plane was much lower than that for the {110} plane.

Fig. 3 shows SEM images of the surface of the same U-shaped diamond trench with vertical {111} sidewalls as that shown in Figs. 1(b) and 2(a): (a) top view, (b) quarter view, and (C) enlarged view of the area enclosed by the white dashed line in Fig. 3(b). The vertical {111} sidewalls had relatively rough surfaces, whereas the slanted {111} sidewalls had smooth surfaces. This difference in sidewall roughness was likely caused by the difference of the contact time with Ni per unit area, i.e., the etching time per unit area. The etching time per unit area for the slanted {111} sidewalls was sufficient because the Ni film was consistently present on almost all areas of them during the etching process. However, the etching time per unit area for the vertical {111} sidewalls was insufficient because the Ni film went down with progress of etching and the contact between Ni film and each area on the vertical {111} sidewalls was maintained for only a short time compared to that on the slanted {111} sidewalls.

Therefore, the vertical {111} sidewalls had a rough surface compared with the slanted {111} sidewalls. With the use of thicker Ni films, smoother vertical {111} sidewalls might be obtained because the etching time can be extended.

Fig. 4 shows 3D LM images of the sample surface morphology (a) after formation of a Ni film with a diameter of 200 μm on the diamond (110) surface and (b) after water-vapor annealing at 1000 °C for 8 min and removal of the deposited film. After the etching process, a diamond trench with a maximum depth of ~50 μm was formed. The shape of the trench was not completely hexagonal on the diamond (110) surface, unlike the one we noticed in Figs. 1(a), 2(b), and 3. In the trench, the slanted {111} sidewalls were not fully extended; thus, a (110) bottom was observed. Judging from these images, this diamond trench should be in its intermediate stage. Hereinafter, a diamond trench with a (110) bottom is referred to as a diamond trench in its intermediate stage. For comparison, a diamond trench with no (110) bottom and surrounded by six {111} sidewalls is referred to as a diamond trench in its final stage.

Fig. 5 shows (a) a 2D LM height image of the surface morphology of the same location shown in Fig. 4b. Fig. 5b, c, and d depicts cross-sectional images corresponding to the line segments CC', DD', and EE'
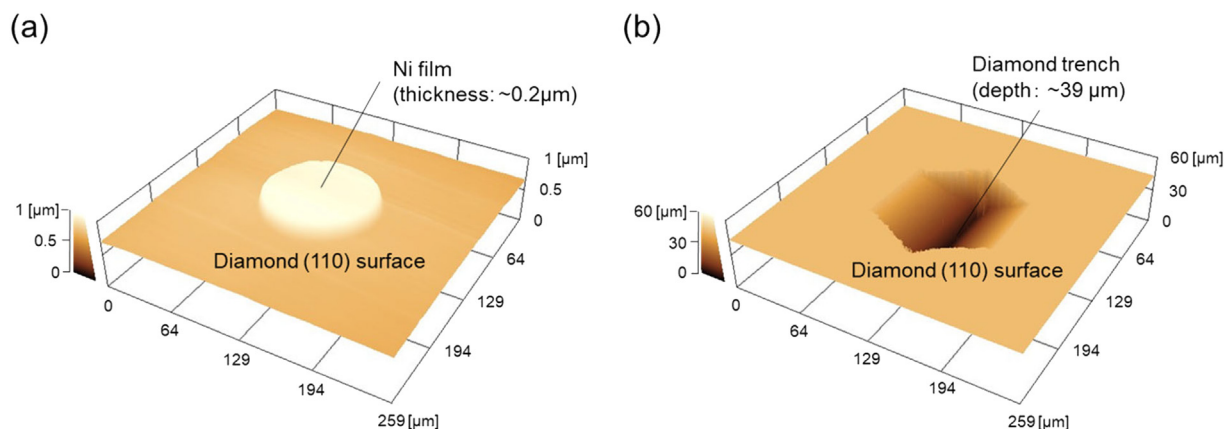
(a)   (b)

Fig. 1. Three-dimensional (3D) LM height images of the sample surface morphology (a) after formation of a Ni film with a diameter of 100 μm on the diamond (110) surface and (b) after water-vapor annealing at 1000 °C for 15 min and removal of the deposited film.
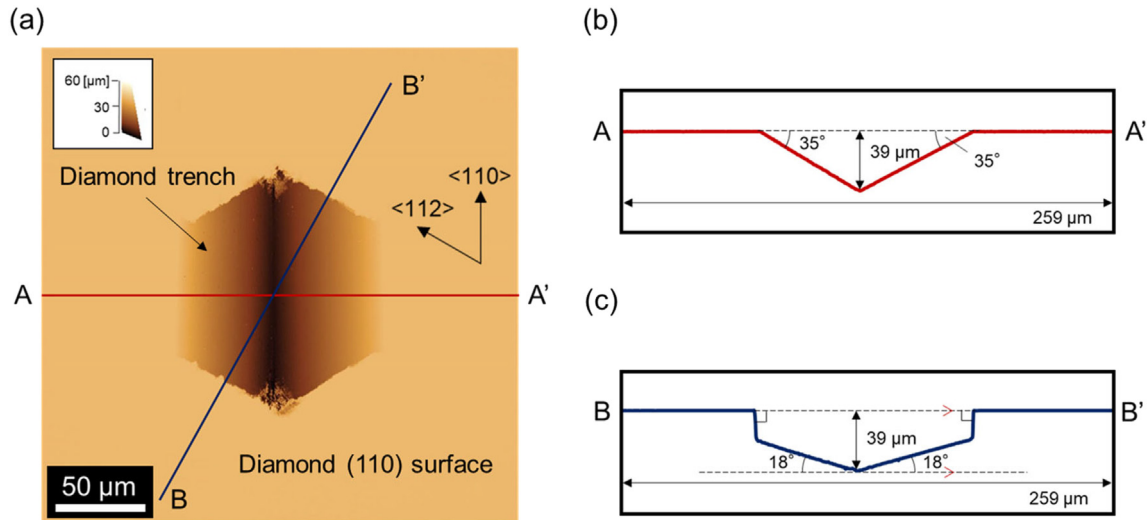
Fig. 2. (a) A two-dimensional (2D) LM height image of the surface morphology at the same location depicted in Fig. 1(b). The line segments AA′ and BB′ in Fig. 2(a) were along the < 100 > and < 111 > directions, respectively. The protrusion structures near the top and bottom of the diamond trench are due to noise. Cross-sectional images corresponding to the line segments (b) AA′ and (c) BB′ in Fig. 2(a).

in Fig. 5(a), respectively. The line segments CC′, DD′, and EE′ in Fig. 5(a) were along the < 100 > direction, the ⟨111⟩ direction, and a direction intermediate between the < 111 > and ⟨110⟩ directions, respectively. As for cross-sectional images corresponding to the lines in the directions of < 100 > and < 111 > , no significant difference was observed compared to those of the diamond trench in its final stage, except for the existence of a (110) bottom. The (110) bottom was rough compared with the initial (110) surface, likely because Ni was deformed by the difference in etching rates between defective areas and non-defective areas during the etching of the polishing damage layer, which includes numerous defects [32]. The cross-sectional image corresponding to the line segment EE′ focuses on the place where the slanted {111} sidewalls do not reach. Therefore, this cross-sectional image is almost equivalent to that corresponding to the line segment DD′ in an earlier stage.

Fig. 6 shows etching depth as a function of water-vapor annealing time at 1000 °C with an approximated straight line. The intercept on the vertical axis (etching depth at 0 min) indicates that etching occurred as the temperature was both raised and lowered. Only the depths of diamond trenches in their intermediate stage, which had (110) bottoms, were used as the etching depth in Fig. 6. The etching rate for diamond

(110) planes in this process was estimated to be 3.8 μm/min on the basis of the slope of the approximated straight line. If the etching rate for (111) is 0, the maximum depth of a trench (D_{max}) is decided by the diameter of Ni film used (D_{Ni}) as the following formula:

$$D_{max} = \frac{D_{Ni} \tan 35°}{2} \simeq 0.35 D_{Ni}. \tag{1}$$

According to the formula, when D_{Ni} is 100 μm, D_{max} should be 35 μm. However, D_{max} of 39 μm was obtained when a Ni film with a diameter of 100 μm was used. Judging from the experimental result, the etching rate for (111) planes is not 0 essentially or because of the presence of crystal defects. The etching depth in the < 111 > directions were determined to be about 2.3 μm from the formula: 4 cos 55 ° . Therefore, considering the etching occurred as the temperature was both raised and lowered, etching rate for (111) planes likely to be < 0.15 μm/min in this case. In addition, because the etching rate for diamond (100) plane in this process is 8.7 μm/min and diamond {111} planes act as etching stopping planes in this process for both (110) and (100) planes, the etching rates of this process decrease in the order [etching rate for (100) plane] > [etching rate for (110) plane] ≫ [etching rate for (111) plane] [26]. Therefore, the anisotropy
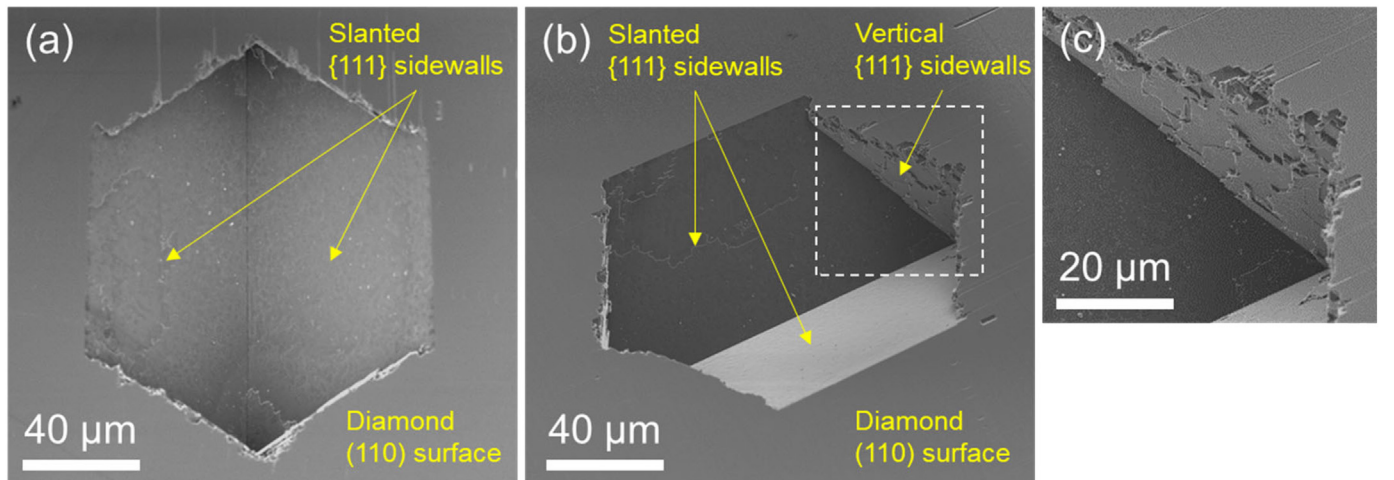

Fig. 3. SEM images of the surface of the same U-shaped diamond trench with vertical {111} sidewalls shown in Figs. 1(b) and 2(a): (a) top view, (b) quarter view, and (c) enlarged view of the area enclosed by the white dashed line in Fig. 3(b).
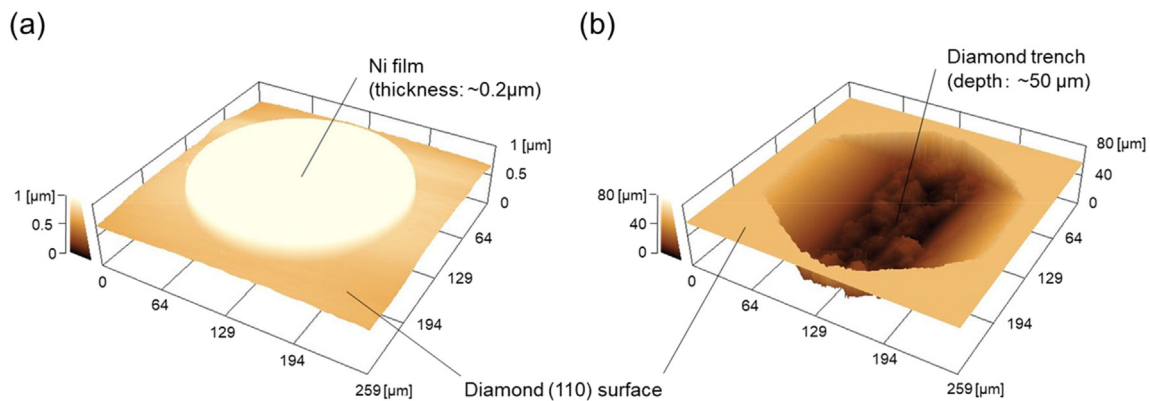
Fig. 4. 3D LM images of the sample surface morphology (a) after formation of a Ni film with a diameter of 200 μm onto a diamond (110) surface and (b) after water-vapor annealing at 1000 °C for 8 min and the removal of the deposited film, respectively.

of this process is similar to those of ethylene diamine pyrocatechol (EDP) and potassium hydroxide (KOH) with isopropyl alcohol (IPA) processes rather than those of KOH and tetra-methyl-ammonium hydroxide (TMAH) processes in terms of Si wet etching processes [19,33,34].

Fig. 7 shows a schematic explaining the formation mechanism of the U-shaped diamond trenches composed of {111} sidewalls via anisotropic etching of diamond (110) surfaces using circular Ni films in high-temperature (1000 °C) water vapor. The top views and the cross-sectional images in the schematic are equivalent to the experimental results already shown in the present paper. The equivalent experimental results are shown in parentheses in Fig. 7. The mechanism is described as follows: The diamond directly under the circular Ni film is etched to form a circular diamond trench. From two tangents of the circular diamond trench in the < 110 > direction, two slanted {111} sidewalls intersecting the diamond (110) surface at 35° start to extend toward the inside of the trench (Fig. 7a). The (110) bottom of the trench gradually disappears as etching progresses and the two slanted {111} sidewalls are extended (Fig. 7b). Finally, the two slanted {111} sidewalls meet just below the center line between the two tangents (Fig. 7c). At the same time, the Ni film expands because of heat and oxidation during crystal anisotropic etching. Accordingly, the slanted {111} sidewalls and vertical {111} sidewalls extend beyond the area where they
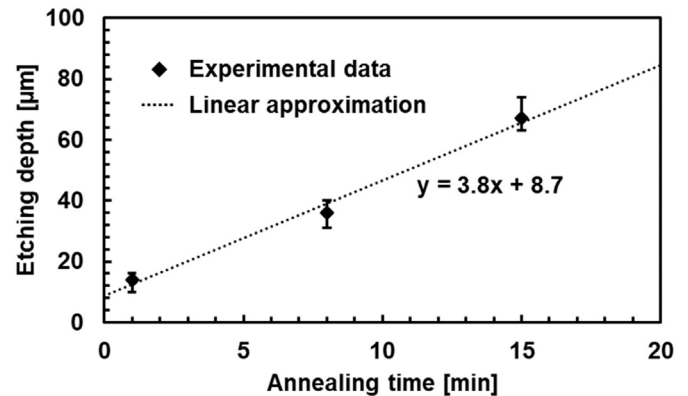

Fig. 6. Etching depth as a function of water-vapor annealing time at 1000 °C with an approximated straight line. The intercepts on the vertical axes (etching depth at 0 min) indicate that etching as the temperature was raised and lowered.

initially contact the Ni film (Fig. 7a). As the etching progresses, the vertical {111} sidewalls are gradually formed toward the inside of the trench from the tangents (Fig. 7b). Finally, the hexagonal trench surrounded by six {111} sidewalls is formed (Fig. 7c).
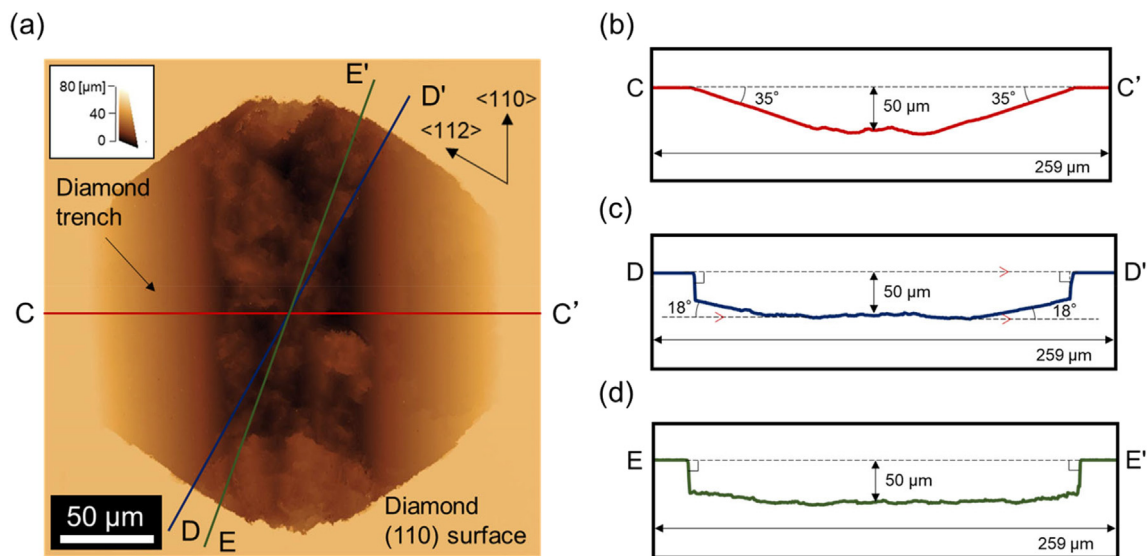

Fig. 5. (a) 2D LM height image of the surface morphology at the same location represented in Fig. 4(b). The line segments CC′, DD′, and EE′ in panel (a) are drawn along the < 100 > direction, the < 111 > direction and in a direction between the < 111 > and a < 110 > directions, respectively. Cross-sectional images corresponding to the line segments (b) CC′, (c) DD′, and (d) EE′ in panel (a).
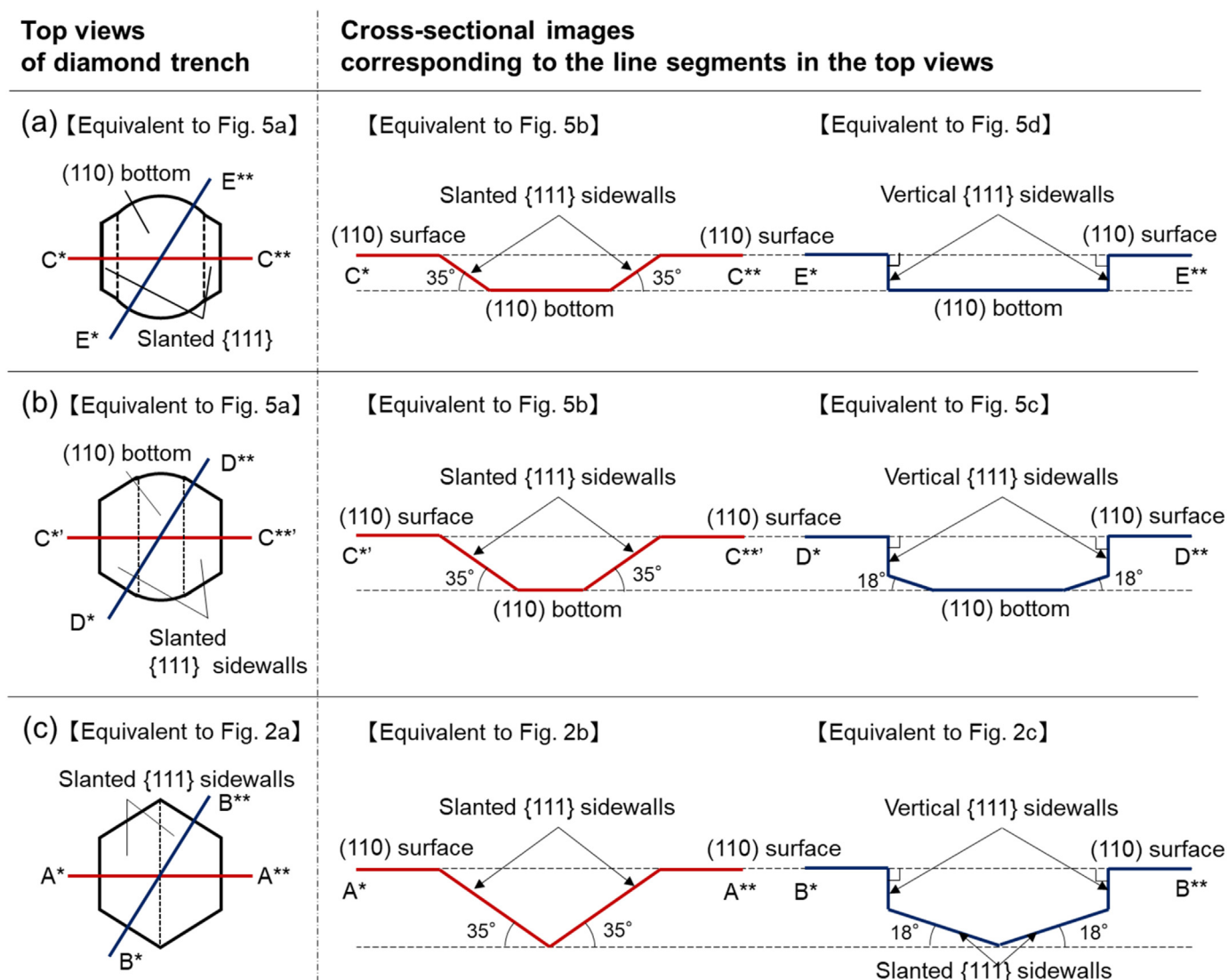
Fig. 7. A schematic explaining the formation mechanism of the U-shaped diamond trenches composed of the {111} sidewalls via anisotropic etching of diamond (110) surfaces using circular Ni films in high-temperature (1000 °C) water vapor.

4. Conclusions

U-shaped diamond trenches with vertical {111} sidewalls were successfully fabricated by applying anisotropic diamond etching using circle Ni films in high-temperature (1000 °C) water vapor for diamond (110) surfaces. The diamond trench in its final stage was hexagonal on the (110) surface and surrounded by six {111} sidewalls (four vertical and two slanted {111} sidewalls to the (110) surface). This observation indicates that the {111} planes function as etching stopping planes and that the etching rate of {111} is much lower than that of (110). The etching rate for diamond (110) surfaces of this process was also estimated to be 3.8 μm/min from the relationship between etching time and etching depth of diamond trenches in their intermediate stages, which had (110) bottoms.

This process enables the fabrication of high-density diamond trenches due to vertical etching and might be useful for cutting diamond wafers if the etching rate is further increased.

CRediT authorship contribution statement

M. Nagai: Conceptualization, Methodology, Validation, Formal analysis, Investigation, Writing - original draft, Visualization, Funding acquisition.**Y. Nakamura:**Investigation, Writing - review & editing.**T. Yamada:**Investigation, Writing - review & editing.**T. Tabakoya:**Writing - review & editing.**T. Matsumoto:**Writing - review & editing.**T. Inokuma:**Resources, Writing - review & editing.**C.E. Nebel:**Writing - review & editing.**T. Makino:**Investigation, Resources, Writing - review & editing.**S. Yamasaki:**Writing - review & editing.**N. Tokuda:**Conceptualization, Methodology, Resources, Writing - review & editing, Supervision, Project administration, Funding acquisition.

Declaration of competing interest

The authors declare that they have no known competing financial interests or personal relationships that could have appeared to influence the work reported in this paper.

Acknowledgments

References

[1] C.J.H. Wort, R.S. Balmer, Diamond as an electronic material, Mater. Today 11 (2008) 22–28, https://doi.org/10.1016/S1369-7021(07)70349-8.

[2] N. Oi, M. Inaba, S. Okubo, I. Tsuyuzaki, T. Kageura, S. Onoda, A. Hiraiwa, H. Kawarada, Vertical-type two-dimensional hole gas diamond metal oxide semiconductor field-effect transistors, Sci. Rep. 8 (2018) 10660, , https://doi.org/10.1038/s41598-018-28837-5.

[3] B. Huang, X. Bai, S.K. Lam, K.K. Tsang, Diamond FinFET without hydrogen termination, Sci. Rep. 8 (2018) 3063, https://doi.org/10.1038/s41598-018-20803-5.

[4] T. Matsumoto, H. Kato, K. Oyama, T. Makino, M. Ogura, D. Takeuchi, T. Inokuma, N. Tokuda, S. Yamasaki, Inversion channel diamond metal-oxide-semiconductor field-effect transistor with normally off characteristics, Sci. Rep. 6 (2016) 31585, , https://doi.org/10.1038/srep31585.

[5] T. Matsumoto, T. Mukose, T. Makino, D. Takeuchi, S. Yamasaki, T. Inokuma, N. Tokuda, Diamond Schottky-pn diode using lightly nitrogen-doped layer, Diam. Relat. Mat. 75 (2017) 152–154, https://doi.org/10.1016/j.diamond.2017.03.018.

[6] T. Matsumoto, H. Kato, T. Makino, M. Ogura, D. Takeuchi, S. Yamasaki, M. Imura, A. Ueda, T. Inokuma, N. Tokuda, Direct observation of inversion capacitance in p-type diamond MOS capacitors with an electron injection layer, Jpn. J. Appl. Phys. 57 (2018) 04FR01, https://doi.org/10.7567/JJAP.57.04FR01.

[7] G. Balasubramanian, P. Neumann, D. Twitchen, M. Markham, R. Kolesov, N. Mizuochi, J. Isoya, J. Achard, J. Beck, J. Tissler, V. Jacques, P.R. Hemmer, F. Jelezko, J. Wrachtrup, Ultralong spin coherence time in isotopically engineered diamond, Nat. Mater. 8 (2009) 383–387, https://doi.org/10.1038/nmat2420.

[8] T.M. Babinec, B.J.M. Hausmann, M. Khan, Y. Zhang, J.R. Maze, P.R. Hemmer, M. Lončar, A diamond nanowire single-photon source, Nat. Nanotechnol. 5 (2010) 195–199, https://doi.org/10.1038/nnano.2010.6.

[9] N. Mizuochi, T. Makino, H. Kato, D. Takeuchi, M. Ogura, H. Okushi, M. Nothaft, P. Neumann, A. Gali, F. Jelezko, J. Wrachtrup, S. Yamasaki, Electrically driven single-photon source at room temperature in diamond, Nat. Photonics 6 (2012) 299–303, https://doi.org/10.1038/nphoton.2012.75.

[10] Y. Tao, J.M. Boss, B.A. Moores, C.L. Degen, Single-crystal diamond nanomechanical resonators with quality factors exceeding one million, Nat. Commun. 5 (2014) 3638, https://doi.org/10.1038/ncomms4638.

[11] M.J. Burek, Y. Chu, M.S.Z. Liddy, P. Patel, J. Rochman, S. Meesala, W. Hong, Q. Quan, M.D. Lukin, M. Lončar, High quality-factor optical nanocavities in bulk single-crystal diamond, Nat. Commun. 5 (2014) 5718, https://doi.org/10.1038/ncomms6718.

[12] B.J.M. Hausmann, I. Bulu, V. Venkataraman, P. Deotare, M. Lončar, Diamond nonlinear photonics, Nat. Photonics 8 (2014) 369–374, https://doi.org/10.1038/nphoton.2014.72.

[13] J. Brugger, G. Beljakovic, M. Despont, N.F. de Rooij, P. Vettiger, Silicon micro/nanomechanical device fabrication based on focused ion beam surface modification and KOH etching, Microelectron. Eng. 35 (1997) 401–404, https://doi.org/10.1016/S0167-9317(96)00210-9.

[14] K. Sato, Fabrication methods based on wet etching process for the realization of silicon MEMS structures with new shapes, Microsyst. Technol. 16 (2010) 1165–1174, https://doi.org/10.1007/s00542-009-0956-5.

[15] X.T. Vu, R. GhoshMoulick, J.F. Eschermann, R. Stockmann, A. Offenhäusser, S. Ingebrandt, Fabrication and application of silicon nanowire transistor arrays forbiomolecular detection, Sensor Actuat. B-Chem. 144 (2010) 354–360, https://doi.org/10.1016/j.snb.2008.11.048.

[16] Y. Liu, K. Ishii, T. Tsutsumi, M. Masahara, E. Suzuki, Ideal rectangular cross-section Si-Fin channel double-gate MOSFETs fabricated using orientation-dependent wet etching, IEEE Electron Device Lett 24 (2003) 484–486, https://doi.org/10.1109/LED.2003.815004.

[17] J.W. Weigold, W.H. Juan, S.W. Pang, Etching and boron diffusion of high aspect ratio Si trenches for released resonators, J. Vac. Sci. Technol. B Microelectron. Nanometer. Struct. Process Meas. Phenom. 15 (1997) 267, https://doi.org/10.1116/1.589276.

[18] V. Karanassios, G. Mew, Anisotropic wet chemical etching of Si for chemical analysis applications, Sens. Mater. 9 (1997) 395–416 https://myukk.org/SM2017/sm_pdf/SM301.pdf.

[19] K. Sato, M. Shikida, Y. Matsushima, T. Yamashiro, K. Asaumi, Y. Iriye, M. Yamamoto, Characterization of orientation-dependent etching properties of single-crystal silicon: effects of KOH concentration, Sens. Actuator A-Phys. 61 (1998) 87–93, https://doi.org/10.1016/S0924-4247(97)01658-0.

[20] G.J. Parker, M.D.B. Charlton, M.E. Zoorob, J.J. Baumberg, M.C. Netti, T. Lee, Highly engineered mesoporous structures for optical processing, Phil. Trans. R. Soc. A 364 (2016) 189–199.

[21] M.J. Archer, F.S. Ligler, Fabrication and characterization of silicon micro-funnels and taped micro-channels for stochastic sensing applications, Sensors 8 (2008) 3848–3872, https://doi.org/10.3390/s8063848.

[22] K. Sato, M. Shikida, T. Yamashiro, K. Asaumi, Y. Iriye, M. Yamamoto, Anisotropic etching rates of single-crystal silicon for TMAH water solution as a function of crystallographic orientation, Sens. Actuator A-Phys. 73 (1999) 131–137, https://doi.org/10.1016/S0924-4247(98)00271-4.

[23] R.E. Oosterbroek, J.W. Berenschot, H.V. Jansen, A.J. Nijdam, G. Pandraud, A. van den Berg, M.C. Elwenspoek, Etching methodologies in < 111 > -oriented silicon wafers, J. Microelectromech. Syst. 9 (2000) 390–398.

[24] P. Pal, K. Sato, A comprehensive review on convex and concave corners in silicon bulk micromachining based on anisotropic wet chemical etching, Micro and Nano Systems Letters 3 (2015) 6, https://doi.org/10.1186/s40486-015-0012-4.

[25] H. Kuroshima, T. Makino, S. Yamasaki, T. Matsumoto, T. Inokuma, N. Tokuda, Mechanism of anisotropic etching on diamond (111) surfaces by a hydrogen plasma treatment, Appl. Surf. Sci. 422 (2017) 452–455, https://doi.org/10.1016/j.apsusc.2017.06.005.

[26] O.A. Ivanov, A.B. Muchnikov, V.V. Chernov, S.A. Bogdanov, A.L. Vikharev, J.E. Butler, Experimental study of hydrogen plasma etching of (100) single crystal diamond in a MPACVD reactor, Mater. Lett. 151 (2015) 115–118, https://doi.org/10.1016/j.matlet.2015.03.073.

[27] M. Nagase, K. Watanabe, H. Umezawa, S. Shikata, Selective-area growth of thick diamond films using chemically stable masks of Ru/Au and Mo/Au, Jpn. J. Appl. Phys. 51 (2012) 070202.

[28] M. Nagai, K. Nakanishi, H. Takahashi, H. Kato, T. Makino, S. Yamasaki, T. Matsumoto, T. Inokuma, N. Tokuda, Anisotropic diamond etching through thermochemical reaction between Ni and diamond in high-temperature water vapour, Sci. Rep. 8 (2018) 6687, https://doi.org/10.1038/s41598-018-25193-2.

[29] M. Nagai, R. Yoshida, T. Yamada, T. Tabakoya, C.E. Nebel, S. Yamasaki, T. Makino, T. Matsumoto, T. Inokuma, N. Tokuda, Conductive-probe atomic force microscopy and Kelvin-probe force microscopy characterization of OH-terminated diamond (111) surfaces with step-terrace structures, Jpn. J. Appl. Phys. 58 (2019) SIIB08, https://doi.org/10.7567/1347-4065/ab1b5c.

[30] S.A. Suliman, N. Gollagunta, L. Trabzon, J. Hao, R.S. Ridley, C.M. Knoedler, G.M. Dolny, O.O. Awadelkarim, S.J. Fonash, The dependence of UMOSFET characteristics and reliability on geometry and processing, Semicond. Sci. Technol. 16 (2001) 447–454, https://doi.org/10.1088/0268-1242/16/6/305.

[31] S.A. Suliman, B. Venkataraman, C.T. Wu, R.S. Ridley, G.M. Dolny, O.O. Awadelkarim, S.J. Fonash, J. Ruzyllo, Electrical properties of the gate oxide and its interface with Si in U-shaped trench MOS capacitors: the impact of polycrystalline Si doping and oxide composition, Solid State Electron 47 (2003) 899–905, https://doi.org/10.1016/S0038-1101(02)00442-2.

[32] K. Nakanishi, H. Kuroshima, T. Matsumoto, T. Inokuma, N. Tokuda, Atomically flat diamond (100) surface formation by anisotropic etching of solid-solution reaction of carbon into nickel, Diam. Relat. Mater. 68 (2016) 127–130, https://doi.org/10.1016/j.diamond.2016.06.011.

[33] O. Tabata, Anisotropic etching of silicon in TMAH solutions, Sens. Mater. 13 (2001) 271–283 https://myukk.org/SM2017/sm_pdf/SM448.pdf.

[34] K.P. Rola, I. Zubel, Study on etching anisotropy of Si(hkl) planes in solutions with different KOH and isopropyl alcohol concentrations, Mater. Sci-Poland 29 (2011) 278–284, https://doi.org/10.2478/s13536-011-0047-z.